Supplementary Information

Thermal conductivity of the n = 1 – 5 and 10 members of the $(SrTiO_3)_nSrO$ Ruddlesden-Popper superlattices

Molecular-Beam Epitaxy Thin-film Growth

Molecular beams of strontium and titanium were generated using a low-temperature effusion cell and a Ti-Ball™,[1] respectively. The fluxes of both elements were pre-calibrated using a quartz crystal microbalance. A more accurate flux calibration was done by following the reflection high-energy electron diffraction (RHEED) intensity oscillations.[2] Judging from the change of maximum/minimum intensity and the shape of oscillations, the shutter time needed for an absolute monolayer dose of each element is precisely determined. To grow $(SrTiO_3)_nSrO$ phases, both the stoichiometry and each monolayer absolute dose cannot be off by more than 1%. Each of the members in this series has different sequences of SrO and TiO_2 layers. We controlled the shutter ordering of strontium and titanium ions to match the layering sequence of the desired (001)-oriented $(SrTiO_3)_nSrO$ phases. All films were grown in an oxidant background pressure (O_2 + ~10% O_3) of 7×10^{-7} Torr at a substrate temperature of 850 °C (as measured by a thermocouple that is not in direct contact with the substrate); the true temperature of the substrate is closer to 750 °C.

X-Ray Diffraction Structural Characterization

To assess the quality and epitaxy of the 300 nm thick n = 2-5, and 10 $(SrTiO_3)_nSrO$ films grown on (100) $SrTiO_3$ and the 200 nm thick n = 1 $(SrTiO_3)_nSrO$ films grown on (100) LSAT, rocking curves in ω were measured shown in Fig. S1. All films were found to have full width at half maximums (FWHM) similar to the underlying substrates, indicative of high-quality epitaxial growth. From Fig. 1(a) in the main text the c-axis lattice constants of each member of the series, determined by Nelson-Riley analysis,[3] are found to be 12.63±0.03 Å, 20.29±0.01 Å, 28.16±0.02 Å, 35.84±0.03 Å, 43.68±0.02 Å, and 82.90±0.02 Å for the n = 1 (LSAT), 2, 3, 4, 5, and 10 phases, respectively. These values are similar to prior Ruddlesden-Popper films grown on (001) $SrTiO_3$ (Ref. 4) and (001) LSAT (Ref. 5).

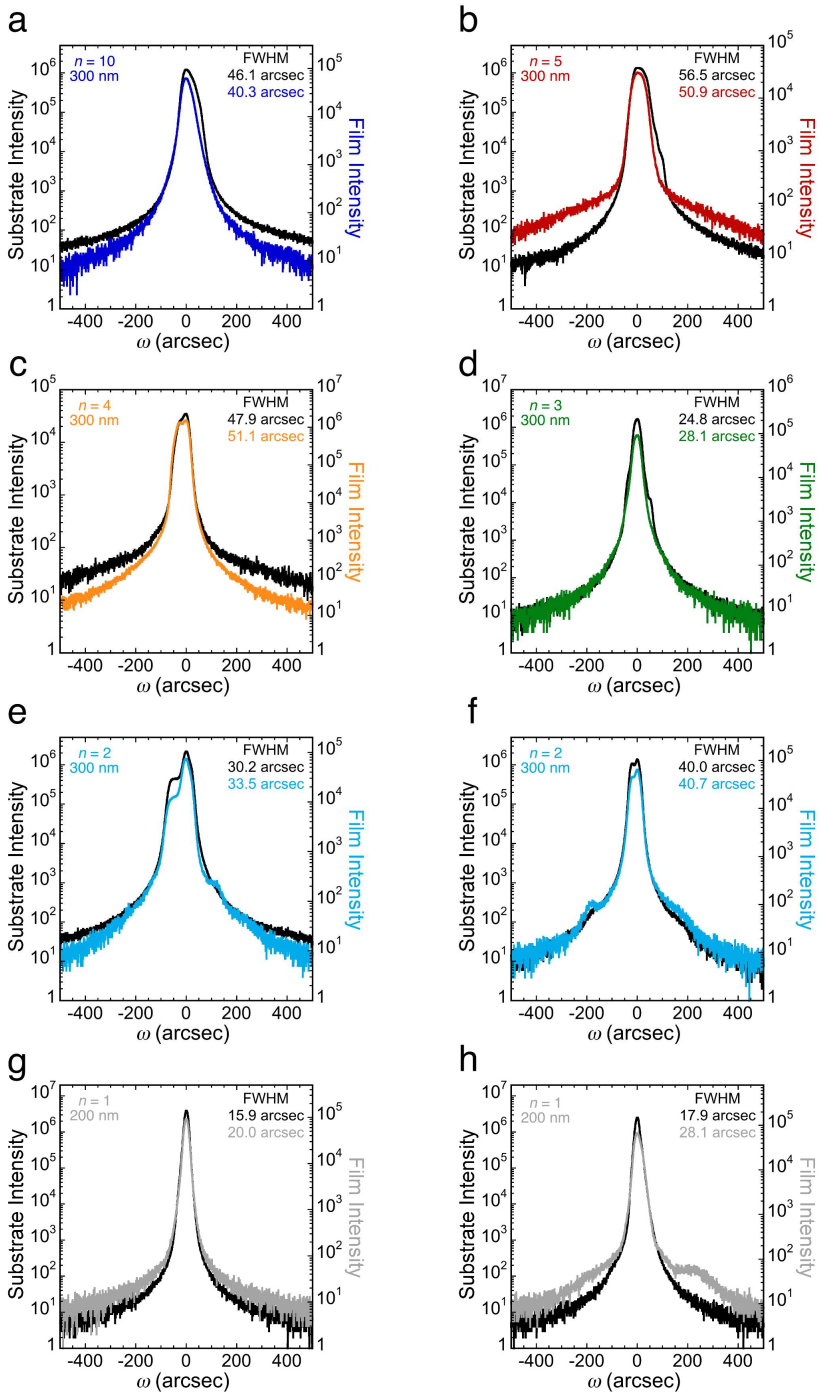

FIG. S1. ω rocking curves of the 300 nm thick n = 2-5, and 10 $(SrTiO_3)_nSrO$ films grown on (100) $SrTiO_3$ (a)-(f) and the 200 nm thick n = 1 $(SrTiO_3)_nSrO$ films grown on (100) LSAT (g) and (h). Superimposed XRD rocking curves of the 002 peaks of the $SrTiO_3$ or LSAT substrate (shown in black) and selected film peaks of the $(SrTiO_3)_nSrO$ n = 1 - 5, and 10 films: (a) n = 10 (00<u>42</u> peak, blue). (b) n = 5 (00<u>22</u> peak, red). (c) n = 4 (00<u>18</u> peak, orange). (d) n = 3 (00<u>14</u> peak, green). (e) n = 2 (00<u>10</u> peak, light blue). (f) n = 2 (00<u>10</u> peak, light blue). (**g**) n = 1 (006 peak, gray). (h) n = 1 (006 peak, gray). The full width at half maximum (FWHM) is given as a measure of crystalline quality for the substrate and film peaks.

Time-domain Thermoreflectance (TDTR) Measurements

Analysis of the TDTR data requires the heat capacities per unit volume of the thin film and the substrate. In cases where no published data of a material's heat capacity was available, we used the heat capacity of chemically and structurally similar phases to analyze the data. For $(SrTiO_3)_nSrO$, the temperature-dependent heat capacities were obtained by using the rule of mixtures to calculate the volumetric average of $SrTiO_3$ and SrO based on the index number *n*. Any systematic errors introduced by uncertainties in the heat capacity in TDTR are smaller than the other uncertainties in the experiment.

To measure TDTR at various temperature, samples were annealed at 300 °C for 30 minutes in order to remove any leftover organic residue on the surface of the sample. The samples were then coated with a 60–70 nm thick Al transducer layer using DC magnetron sputtering. The measurement was done using a single microscope objective lens, with a focused spot size of 10.7 μm. The power of the laser was controlled so that the steady-state temperature increase from the laser heating is less than 10 K. The thermal conductivity of the substrate was taken from the literature for LSAT[6] or was measured experimentally from single-crystal $SrTiO_3$ substrates.

Ab Initio Calculations

We performed fully *ab initio* calculations of the thermal conductivity in the Ruddlesden-Popper phases via the full solution of the Boltzmann transport equation (BTE)[7] within cubic anharmonicity. We obtained second- and third-order force constants via the temperature-dependent effective potential scheme by fitting the force constants to the forces produced during short *ab initio* molecular dynamics (AIMD) runs.[8] We adopted this approach since $SrTiO_3$ is dynamically stabilized in the cubic structure, and thus within the standard harmonic approximation the phonon spectrum features imaginary frequencies.[9] *Ab initio* molecular dynamics (AIMD) runs were performed for the total of 2000 time steps of 1 fs at 300 K by preparing 20 initial configurations drawn from a canonical distribution and

propagated for 100 time steps. This dataset features statistically independent set of forces and positions, appropriate for force constants fitting. The quality of each dataset was assessed by sampling different atomic configurations for force fitting and the results shows negligible differences between different samples. In VASP, the PBESol density functional[10] was adopted, with a 500 eV energy cutoff of the plane-wave expansion of the wavefunctions. The in-plane lattice constants of the simulated $(SrTiO_3)_nSrO$ phases were fixed to the corresponding substrate on which the material was grown, while the out-of-plane lattice constant (the *c*-axis of each $(SrTiO_3)_nSrO$ phase) was optimized. Primitive-cell calculations were performed with k-grid resolution of 6×6×6, while all AIMD runs were carried out at the Gamma point only on supercells ranging from 3×3×3 for $SrTiO_3$ to 3×3×1 for $Sr_5Ti_4O_{13}$. The distance cutoffs for second- and third-order force constants were 5 A and 4.5 A, respectively, and we neglected electrostatic long-range contributions to the phonons, *i.e.*, the spectrum does not feature splitting of the longitudinal and transverse optical phonons. We further assumed that the force constants are only weakly temperature-dependent in the range relevant for the experimental observations, and thus we used resultant force constants to calculate the thermal conductivity in the 150-500 K range for comparison with the experimental data. The phonon mean free path for a given compound was estimated as the 50% point of the thermal conductivity accumulation function.

References

1. C. D. Theis and D. G. Schlom, J. Vac. Sci. Technol. A **14**, 2677 (1996).
2. J. H. Haeni, C. D. Theis, and D. G. Schlom, J. Electroceram. **4**, 385 (2000).
3. J. B. Nelson and D. P. Riley, Proc. Phys. Soc. London **57**, 160 (1945).
4. J. H. Haeni, C. D. Theis, D. G. Schlom, W. Tian, X. Q. Pan, H. Chang, I. Takeuchi, and X.-D. Xiang, Appl. Phys. Lett. **78**, 3292 (2001).

5. C. H. Lee, N. J. Podraza, Y. Zhu, R. F. Berger, S. Shen, M. Sestak, R. W. Collins, L. F. Kourkoutis, J. A. Mundy, H. Q. Wang, Q. Mao, X. X. Xi, L. J. Brillson, J. B. Neaton, D. A. Muller, and D. G. Schlom, Appl. Phys. Lett. **102** 122901 (2013).

6. J. Hidde, C. Guguschew, S. Ganschow, D. Klimm, J. Alloy Compd. **738**, 415 (2018).

7. A. Ward, D. A. Broido, D. A. Stewart, and G. Deinzer, Phys. Rev. B. **80**, 125203 (2009).

8. O. Hellman and I. A. Abrikosov, Phys. Rev. B **88**, 144301 (2013).

9. J.-J. Zhou, O. Hellman, and M. Bernardi, Phys. Rev. Lett. **121**, 226603 (2018).

10. G. I. Csonka, J. P. Perdew, A. Ruzsinszky, P. H. T. Philipsen, S. Lebègue, J. Paier, O. A. Vydrov, and J. G. Ángyán, Phys. Rev. B **79**, 155107 (2019).